Surface waves generated by an oscillating circular cylinder on water of finite depth: theory and experiment

By Y. S. YU
Department of Engineering Mechanics, University of Kansas

AND F. URSELL
Department of Applied Mathematics and Theoretical Physics, University of Cambridge

(Received 2 March 1961)

The mean position of the cylinder is in the mean free surface, and the cylinder is oscillating vertically (heaving) with a simple harmonic motion of small amplitude. The problem is studied both theoretically and experimentally. The present paper may be regarded as a sequel to an earlier paper (Ursell, Dean & Yu 1959) on the waves due to a piston wave-maker.

The theory is based upon the usual assumptions of classical hydrodynamics, i.e. that the fluid is inviscid and of uniform density, and that motion starts from rest; the motion is then irrotational. Non-linear terms in the equations of motion are neglected. It is also assumed that the motion is two-dimensional and that the wave channel is of infinite length in both horizontal directions normal to the axis of the cylinder. The solution of the boundary-value problem is written as the sum of a series of certain wave potentials where the coefficients satisfy an infinite number of linear equations in an infinite number of unknowns. This theory is an extension to finite constant depth of the known theory (Ursell 1949) for infinite depth. Computations are presented for the wave amplitude at infinity and for the virtual-mass coefficient for $h/a = 2$, 4, 10 and ∞, where h is the water depth and a is the radius of the cylinder.

The experiments were conducted in a 100 ft. wave channel, and were arranged to be two-dimensional and symmetrical about the vertical plane through the axis of the cylinder. The waves generated by the heaving cylinder were partially absorbed and partially reflected at the ends of the wave channel. The results of measurement thus depend on the precise length of the channel and the accuracy is low unless the effect of reflexion can be allowed for, as was done in the earlier wave-maker experiment. A more elaborate method of measurement and analysis is developed here for the heaving cylinder, to give the amplitude which would have been observed in a wave channel of infinite length. Use is made of the symmetry of the experimental arrangement. Several improvements made in the technique of measurement since the wave-maker experiment are reported.

Comparison of theory and experiment for the wave amplitude shows good

agreement, the experimental values being in general a few percent lower than the theoretical values. This provides much-needed evidence for the practical values of the linearized theory of water waves.

1. Introduction

The greater part of the mathematical theory of water waves is based on the following assumptions: (1) Density variations and viscosity in the fluid are negligible; the motion, if originally started from rest, is then irrotational and can be described by a velocity potential. (2) Non-linear terms in the equations of motion are negligible; this seems reasonable if the amplitude of motion is small enough. It is important to know in what circumstances the linearized theory agrees with experimental measurements. Any such agreement is confirmation both of the practical value of the theory and the validity of the experimental technique; and where agreement between theory and experiment is established or expected, it may well be simpler to use theory rather than experiment. The experimental evidence relating to the linearized theory was discussed by Ursell *et al.* (1959, §2; this paper will henceforth be referred to as I), who pointed out that up to 1959 almost all the evidence in favour of the theory related to frequencies and velocities, rather than to wave forces and wave heights about which there was serious doubt. More conclusive evidence was provided by their experiment on the height of waves generated by a flat vertical piston wave-maker. They obtained very good agreement with the linearized theory for small waves (and also a systematic deviation for higher waves for which no theory is available). In their experiment all the assumptions of the theory were simulated, except that the absorption of waves at the end of the wave channel was incomplete. (Unfortunately, all known wave absorbers reflect a considerable proportion of the wave amplitude, and so all measurements depend on the precise length of the wave channel. The common failure to allow for incomplete reflexion implies a serious limitation on the accuracy of laboratory wave measurement.) They developed a method of allowing for incomplete absorption in their experiments, and the good results obtained by them depended on this. They also assumed that the wave-maker reflected waves incident on it from the absorber like a fixed rigid wall; this follows from the linearized theory for the piston wave-maker and greatly simplifies the analysis of the experiments. This simplified analysis is valid only for a nearly vertical wave-maker, however.

The present study is concerned with a configuration of both greater complexity and greater practical interest than a piston wave-maker. A circular horizontal cylinder has its mean position in the mean free surface of the wave channel and makes periodic heaving (i.e. vertical) oscillations. The theory is known for a wave channel of infinite depth (Ursell 1949). It is here extended to a wave channel of finite constant depth, computed and compared with measurements.

In §2 below, the (two-dimensional) theory for finite depth is given. This problem involves two dimensionless parameters (based on cylinder radius, water depth, and wavelength), whereas the theory for infinite depth involves only one. The wave amplitude and force on the heaving cylinder are computed when the

absorption at the ends of the wave channel is assumed complete. In §3 the experimental arrangement for measuring the wave amplitude is described. An effort was made to make the experiment symmetrical about the vertical plane through the axis of the cylinder. The absorption at the ends of the wave channel is again incomplete in these experiments; a method of analysing the measurements to allow for this is developed in §4. Theory and experiment for the wave amplitude are compared in §5, and it will be seen that the agreement is close. (No measurements of forces have yet been made; see, however, Porter 1960.)

2. Mathematical theory

The mathematical boundary-value problem, assumed two-dimensional, is formulated as follows (cf. Ursell 1949).

The origin of co-ordinates is taken at the mean position of the centre of the heaving circle (the horizontal projection of the cylinder), the equation of the mean free surface is $y = 0$, and the equation of the bottom is $y = h > 0$. Polar co-ordinates are defined† by $x = r\sin\theta$, $y = r\cos\theta$, the equation of the mean position of the moving circle being $r = a$. The motion is periodic with period $2\pi/\sigma$. Then the velocity potential $\Phi(x, y; t)$ satisfies

$$\left(\frac{\partial^2}{\partial x^2}+\frac{\partial^2}{\partial y^2}\right)\Phi(x,y;t) = 0 \quad \text{in} \quad -\infty < x < \infty, \quad 0 < y < h, \quad r > a. \tag{2.1}$$

The boundary conditions are

$$K\Phi+\frac{\partial\Phi}{\partial y} = 0 \quad \text{on} \quad y = 0, \quad r > a, \tag{2.2}$$

where $K = \sigma^2/g$, and

$$\frac{\partial\Phi}{\partial y} = 0 \quad \text{on} \quad y = h. \tag{2.3}$$

Also, there is the 'radiation condition' that at infinity the waves travel outwards; and further

$$\frac{\partial\Phi}{\partial r} = U(t)\cos\theta \quad \text{on} \quad r = a, \tag{2.4}$$

where $U(t)$ is the simple-harmonic vertical velocity of the centre of the moving circle. Since the problem is linear, the potential is proportional to $U(t)$, and it is convenient not to prescribe the amplitude and phase of $U(t)$ at this stage (see equation (2.27) below). The radiation condition is satisfied only approximately in our experiments, because of reflexion from the ends of the channel (see §4 below). The downward surface displacement $\eta(x, t)$ is given in terms of the potential Φ by

$$\eta = \frac{1}{g}\frac{\partial}{\partial t}\Phi(x, 0; t), \tag{2.5}$$

and the pressure $p(x, y; t)$ by

$$p = \rho g y - \rho\frac{\partial\Phi}{\partial t}. \tag{2.6}$$

With the exception of an important paper by John (1950) on fundamental mathematical aspects, all previous work on this problem is concerned with the

† It is convenient, because of the symmetry of the problem, to measure θ from the vertical rather than from the horizontal axis.

special case of infinite depth. The theory and computations given by Ursell (1949) are useful for small and moderate values of Ka, and it is this work which is extended to finite depth in our present paper. In principle this method works

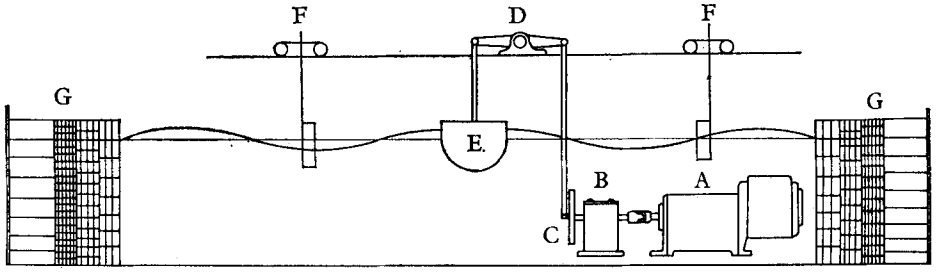

FIGURE 1. Schematic diagram of experimental arrangement. A—variable speed motor, B—reducing gear, C—flywheel, D—lever-type linkage, E—cylinder, F—wave gauges and carriages, G—wave absorbers.

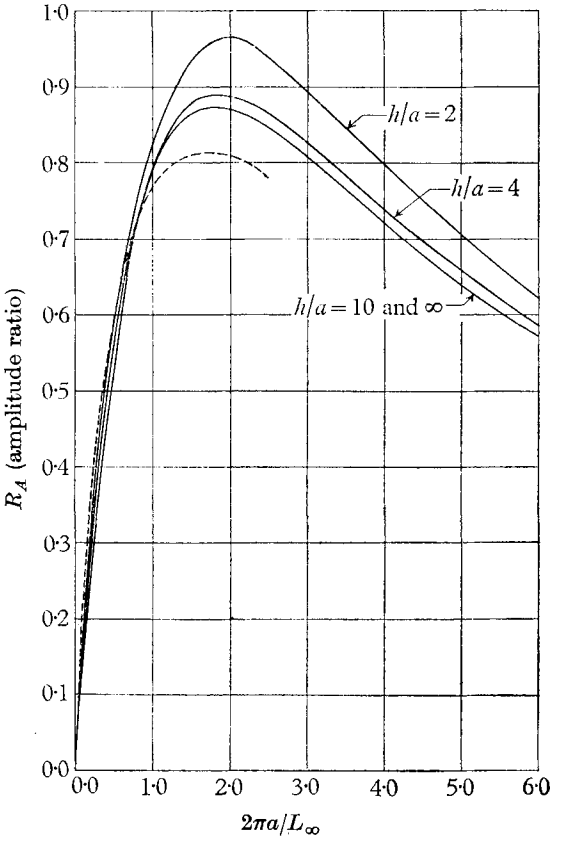

FIGURE 2. Theoretical amplitude ratios. ——, Computed curve; – – – –, Grim's curve $h/a = \infty$.

for all Ka, but actually the equations become ill-conditioned for large Ka, and a different method (Ursell 1953) is then more suitable; this has been used to calculate asymptotic expressions for large Ka for deep water (see also Grim 1953).

An approximate mathematical theory has been given by Grim (1953) who satisfies the boundary conditions on the free surface and on the cylinder only approximately; his results for small and moderate Ka are shown for comparison with ours in figures 2 and 3. A critical discussion of earlier approximations by various authors is given by Ursell (1954).

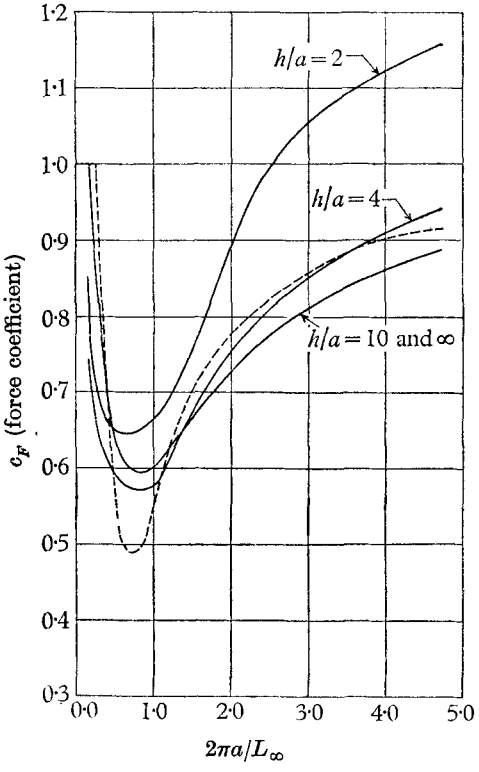

FIGURE 3. Theoretical force coefficients. ——, Computed curve; – – – –, Grim's curve $h/a = \infty$.

In the present paper the potential is written as the sum (with undetermined coefficients) of wave potentials each satisfying equations (2.1) to (2.3) and the radiation condition; the coefficients are to be chosen so that the velocity on the circle is given by (2.4). The wave potentials used by Ursell (1949) for the heaving cylinder on infinitely deep water were (1) a wave-source potential with a multi-valued logarithmic singularity at the origin and (2) single-valued multipole potentials singular at the origin. Analogous wave potentials will now be derived for water of constant finite depth, which reduce to the earlier forms when $h = \infty$. The singular integrals which arise are to be interpreted as Cauchy principal values, and are marked by $\mathscr{P}$ in front of the integral sign; thus

$$\mathscr{P}\int_0^\infty \frac{e^{-ky}\cos kx}{K-k}\,dk = \lim_{\epsilon\to 0}\left[\left(\int_0^{K(1-\epsilon)} + \int_{K(1+\epsilon)}^\infty\right)\frac{e^{-ky}\cos kx}{K-k}\,dk\right].$$

The shallow-water wave-number k_0 is defined by

$$k_0 \tanh k_0 h = K. \tag{2.7}$$

2.1. *The wave-source potential*

This is

$$\mathscr{P}\int_0^\infty \frac{\cosh k(h-y)\cos kx\,dk}{K\cosh kh - k\sinh kh}\cos\sigma t$$

$$-\frac{2\pi\cosh k_0 h}{2k_0 h+\sinh 2k_0 h}\cosh k_0(h-y)\cos k_0 x\sin\sigma t \qquad (2.8)$$

$$= F(x,y)\cos\sigma t + f(x,y)\sin\sigma t, \quad \text{say} \qquad (2.9)$$

(see Thorne 1953, p. 714). Clearly $f(x,y)\sin\sigma t$ is a standing wave, adjusted (as will be seen later) so that the combination satisfies the radiation condition. The expansion near the origin is obtained by noting that

$$F(x,y) = \mathscr{P}\int_0^\infty \frac{e^{-ky}\cos kx}{K-k}\,dk \qquad (2.10)$$

$$+\mathscr{P}\int_0^\infty \frac{e^{-kh}(K\sinh ky - k\cosh ky)\cos kx}{(K-k)(K\cosh kh - k\sinh kh)}\,dk. \qquad (2.11)$$

Now (2.10) is the singular term in the deep-water source potential (Thorne 1953, p. 710), and its expansion is derived in Appendix A; but (2.11) is clearly regular harmonic in $|y| < 2h$. The series expansion of (2.11) is obtained by substituting the expansions

$$\cosh ky\cos kx = \sum_{s=0}^{\infty}\frac{(kr)^{2s}}{(2s)!}\cos 2s\theta,$$

$$\sinh ky\cos kx = \sum_{s=0}^{\infty}\frac{(kr)^{2s+1}}{(2s+1)!}\cos(2s+1)\theta,$$

and inverting the order of summation and integration. Thus

$$F(x,y) = (\gamma+\ln Kr)\sum_{s=0}^{\infty}\frac{(-Kr)^s}{s!}\cos s\theta - \theta\sum_{s=1}^{\infty}\frac{(-Kr)^s}{s!}\sin s\theta$$

$$-\sum_{s=1}^{\infty}\frac{(-Kr)^s}{s!}\left(\frac{1}{1}+\frac{1}{2}+\ldots+\frac{1}{s}\right)\cos s\theta$$

$$+Kh\sum_{s=0}^{\infty}\frac{1}{(2s+1)!}G_{2s+1}(Kh)\left(\frac{r}{h}\right)^{2s+1}\cos(2s+1)\theta$$

$$-\sum_{s=0}^{\infty}\frac{1}{(2s)!}G_{2s+1}(Kh)\left(\frac{r}{h}\right)^{2s}\cos 2s\theta, \qquad (2.12)$$

where by definition

$$G_{2s+1}(v) = \mathscr{P}\int_0^\infty \frac{u^{2s+1}e^{-u}\,du}{(v-u)(v\cosh u - u\sinh u)}, \qquad (2.13)$$

and $\gamma = 0{\cdot}5772\ldots$ is Euler's constant. It can be shown that the wave-source potential (2.8) satisfies the radiation condition. The limit of $F(x,y)$ for large x can be found by noting that the integral

$$\int\frac{\cosh k(h-y)\exp(ik|x|)}{K\cosh kh - k\sinh kh}\,dk$$

along the real k-axis (indented at $k = k_0$, where the integrand has a simple pole) is equal to the integral along $\arg k = \frac{1}{4}\pi$, and thus clearly tends to zero as $|x|$ tends to infinity. Thus

$$\mathscr{P}\int_0^\infty \frac{\cosh k(h-y)\exp(ik|x|)}{K\cosh kh - k\sinh kh}\,dk - \pi i \times (\text{residue at } k = k_0) \to 0 \quad \text{as} \quad |x| \to \infty.$$

(The second term is the finite contribution from the indentation at the pole.) Taking real parts we find that

$$F(x,y) - \frac{2\pi\cosh k_0 h}{2k_0 h + \sinh 2k_0 h}\cosh k_0(h-y)\sin k_0|x| \to 0 \quad \text{as} \quad |x| \to \infty,$$

whence $$F(x,y)\cos\sigma t + f(x,y)\sin\sigma t \tag{2.14}$$

$$-\frac{2\pi\cosh k_0 h}{2k_0 h + \sinh 2k_0 h}\cosh k_0(h-y)\sin(k_0|x| - \sigma t) \to 0; \tag{2.15}$$

and since (2.15) clearly satisfies the radiation condition, the potential (2.14) also does so. Similarly $F(x,y)\sin\sigma t - f(x,y)\cos\sigma t$ satisfies the radiation condition, but we shall not use this function.

2.2. *The multipole potentials*

These are

$$F_{2n}(x,y)\cos\sigma t + f_{2n}(x,y)\sin\sigma t \quad \text{and} \quad F_{2n}(x,y)\sin\sigma t - f_{2n}(x,y)\cos\sigma t,$$

where $F_{2n}(x,y)$ $(n = 1, 2, 3, \ldots)$ is of the form

$$F_{2n}(x,y) = \frac{\cos 2n\theta}{r^{2n}} + \frac{K}{2n-1}\frac{\cos(2n-1)\theta}{r^{2n-1}} \tag{2.16}$$

$$+\int_0^\infty \{c_1^{(2n)}(k)\sinh ky + c_2^{(2n)}(k)\cosh ky\}\cos kx\,dk. \tag{2.17}$$

The terms $f_{2n}(x,y)\cos\sigma t$ and $f_{2n}(x,y)\sin\sigma t$ are standing waves, added so that each complete multipole potential satisfies the radiation condition (cf. §2.1 above). The coefficient functions $c_1^{(2n)}(k)$ and $c_2^{(2n)}(k)$ are chosen so that $F_{2n}(x,y)$ satisfies both the free-surface and the bottom condition. For this purpose it is convenient to use in (2.16) the representation

$$\frac{\cos m\theta}{r^m} = \frac{1}{(m-1)!}\int_0^\infty k^{m-1}e^{-ky}\cos kx\,dk, \tag{2.18}$$

which is valid when $y > 0$ (see Whittaker & Watson 1927, §12.2). It is thus found that

$$F_{2n}(x,y) = \frac{\cos 2n\theta}{r^{2n}} + \frac{K}{2n-1}\frac{\cos(2n-1)\theta}{r^{2n-1}} \tag{2.19}$$

$$+\frac{1}{(2n-1)!}\mathscr{P}\int_0^\infty \frac{e^{-kh}(K+k)(K\sinh ky - k\cosh ky)\,k^{2n-2}\cos kx}{K\cosh kh - k\sinh kh}\,dk, \tag{2.20}$$

and the series expansion of (2.20) can be found in the same way as the expansion of (2.11) above. It is

$$-\frac{h^{-2n}}{(2n-1)!}\sum_{s=0}^{\infty}\frac{1}{(2s)!}\mathscr{F}_{2n+2s-1}(Kh)\left(\frac{r}{h}\right)^{2s}\cos 2s\theta$$

$$+\frac{Kh^{-2n+1}}{(2n-1)!}\sum_{s=0}^{\infty}\frac{1}{(2s+1)!}\mathscr{F}_{2n+2s-1}(Kh)\left(\frac{r}{h}\right)^{2s+1}\cos(2s+1)\theta, \quad (2.21)$$

where by definition

$$\mathscr{F}_{2m-1}(v) = \mathscr{P}\int_0^{\infty}\frac{(v+u)\,u^{2m-1}e^{-u}\,du}{v\cosh u - u\sinh u}. \quad (2.22)$$

The behaviour of $F_{2n}(x,y)$ at infinity can be found, in the same way as the behaviour of $F(x,y)$ above, to be

$$F_{2n}(x,y)+\frac{2\pi k_0^{2n}\cosh k_0(h-y)\sin k_0|x|}{(2n-1)!\cosh k_0 h(2k_0h+\sinh 2k_0h)}\to 0 \quad \text{as} \quad |x|\to\infty. \quad (2.23)$$

Thus, if

$$f_{2n}(x,y) = \frac{2\pi k_0^{2n}\cosh k_0(h-y)\cos k_0 x}{(2n-1)!\cosh k_0 h(2k_0h+\sinh 2k_0h)}, \quad (2.24)$$

the combinations

$$F_{2n}(x,y)\cos\sigma t + f_{2n}(x,y)\sin\sigma t \quad \text{and} \quad F_{2n}(x,y)\sin\sigma t - f_{2n}(x,y)\cos\sigma t$$

satisfy the radiation condition. Note that $F_{2n}(x,y)$ reduces to (2.19) when $h=\infty$, and that $f_{2n}(x,y)$ then vanishes; the multipole potentials are then *wave-free* at infinity.

2.3. *Expansion of the velocity potential*

The velocity potential $\Phi(x,y;t)$ is written in the form $(gb/\pi\sigma J)\,\phi(x,y;t)$, where J is a non-dimensional quantity which is adjusted so that b is the amplitude at infinity. Then $\phi(x,y;t)$ is non-dimensional, and we assume that

$$\phi(x,y;t) = F(x,y)\cos\sigma t + f(x,y)\sin\sigma t \quad (2.25)$$

$$-\sum_{n=1}^{\infty}\frac{a^{2n}}{2n}p_{2n}\{F_{2n}(x,y)\cos\sigma t + f_{2n}(x,y)\sin\sigma t\}$$

$$-\sum_{n=1}^{\infty}\frac{a^{2n}}{2n}q_{2n}\{F_{2n}(x,y)\sin\sigma t - f_{2n}(x,y)\cos\sigma t\}. \quad (2.26)$$

Note that in this expansion the amplitude and phase of the wave-source potential (2.25) have been arbitrarily prescribed. The coefficients p_{2n}, q_{2n} and also the amplitude and phase of the motion of the cylinder are to be found from the boundary condition on the cylinder $r=a$, where the prescribed normal velocity is proportional to $\cos\theta$ (see (2.4) above). We take

$$\frac{\partial\phi}{\partial r} = \frac{1}{a}(A\cos\sigma t + B\sin\sigma t)\cos\theta \quad \text{on} \quad r=a, \quad (2.27)$$

where A and B are additional unknowns. On differentiating the assumed expan-

sion for $\phi(x, y; t)$ and equating coefficients of $\cos \sigma t$ and $\sin \sigma t$, it is seen that in the range $0 < \theta < \frac{1}{2}\pi$ the unknowns must satisfy the simultaneous equations

$$A \cos\theta = \left(a\frac{\partial}{\partial r}F(r,\theta)\right) - \sum_{n=1}^{\infty} \frac{a^{2n}}{2n} p_{2n}\left(a\frac{\partial}{\partial r}F_{2n}(r,\theta)\right) + \sum_{n=1}^{\infty} \frac{a^{2n}}{2n} q_{2n}\left(a\frac{\partial}{\partial r}f_{2n}(r,\theta)\right), \tag{2.28}$$

$$B \cos\theta = \left(a\frac{\partial}{\partial r}f(r,\theta)\right) - \sum_{n=1}^{\infty} \frac{a^{2n}}{2n} p_{2n}\left(a\frac{\partial}{\partial r}f_{2n}(r,\theta)\right) - \sum_{n=1}^{\infty} \frac{a^{2n}}{2n} q_{2n}\left(a\frac{\partial}{\partial r}F_{2n}(r,\theta)\right), \tag{2.29}$$

where, after differentiation, r is put equal to a.

It is convenient to replace these equations by an equivalent infinite set of linear equations in an infinite number of unknowns, obtained (from analogy with a Fourier cosine series) by multiplying (2.28) and (2.29) by the complete set of functions $\cos 2m\theta\,(m = 0, 1, 2, \ldots)$ and integrating from 0 to $\frac{1}{2}\pi$. (When $h = \infty$, the equations for p_{2n} are independent of the equations for q_{2n}.) Thus the equations for $m = 0$ are

$$\begin{aligned} A = {} & \tfrac{1}{2}\pi \cos Ka - (\gamma + \ln Ka)\sin Ka \\ & + \sum_{s=0}^{\infty} (-1)^s \frac{(Ka)^{2s+1}}{(2s+1)!}\left(\frac{1}{1} + \frac{1}{2} + \ldots + \frac{1}{2s+1}\right) + Ka \sum_{n=1}^{\infty} \frac{(-1)^{n+1} p_{2n}}{2n(2n-1)} \\ & + Kh \sum_{s=0}^{\infty} \frac{(-1)^s}{(2s+1)!}\left(\frac{a}{h}\right)^{2s+1} G_{2s+1}(Kh) \\ & - Ka \sum_{s=0}^{\infty} \sum_{n=1}^{\infty} \frac{(-1)^s}{(2n)!\,(2s+1)!}\left(\frac{a}{h}\right)^{2n+2s} p_{2n}\, \mathscr{F}_{2n+2s-1}(Kh) \\ & - \frac{2\pi \sin k_0 a \tanh k_0 h}{2k_0 h + \sinh 2k_0 h} \sum_{n=1}^{\infty} \frac{(k_0 a)^{2n}}{(2n)!} q_{2n}, \end{aligned} \tag{2.30}$$

$$\begin{aligned} B = {} & \frac{\pi \sin k_0 a \sinh 2k_0 h}{2k_0 h + \sinh 2k_0 h} + Ka \sum_{n=1}^{\infty} \frac{(-1)^{n+1} q_{2n}}{2n(2n-1)} \\ & - Ka \sum_{s=0}^{\infty} \sum_{n=1}^{\infty} \frac{(-1)^s}{(2n)!\,(2s+1)!}\left(\frac{a}{h}\right)^{2n+2s} q_{2n}\, \mathscr{F}_{2n+2s-1}(Kh) \\ & + \frac{2\pi \sin k_0 a \tanh k_0 h}{2k_0 h + \sinh 2k_0 h} \sum_{n=1}^{\infty} \frac{(k_0 a)^{2n}}{(2n)!} p_{2n}, \end{aligned} \tag{2.31}$$

where
$$G_{2s+1}(v) = \int_0^{\infty} \frac{u^{2s+1} e^{-u}\, du}{(v-u)(v\cosh u - u \sinh u)},$$

and
$$\mathscr{F}_{2s+1}(v) = \int_0^{\infty} \frac{(u+v)\, u^{2s+1} e^{-u}\, du}{v\cosh u - u \sinh u} = v^2 G_{2s+1}(v) - G_{2s+3}(v).$$

The equations which arise when (2.28) and (2.29) are multiplied by $\cos 2m\theta\,(m > 1)$ and integrated over $(0, \frac{1}{2}\pi)$ are similar but more complicated and will not be written down here. If A and B are eliminated from these by means of (2.30)

and (2.31), the new equations involve only the unknowns p_{2n} and q_{2n}, and are seen to be of the form

$$p_{2m}+\sum_{n=1}^{\infty} a_{mn}p_{2n}+\gamma_m\sum_{n=1}^{\infty}\frac{(k_0a)^{2n}}{(2n)!}q_{2n}=\alpha_m \quad (m=1,2,3,\ldots), \tag{2.32}$$

$$q_{2m}+\sum_{n=1}^{\infty} a_{mn}q_{2n}-\gamma_m\sum_{n=1}^{\infty}\frac{(k_0a)^{2n}}{(2n)!}p_{2n}=\beta_m \quad (m=1,2,3,\ldots), \tag{2.33}$$

where $\alpha_m, \beta_m, \gamma_m$ and a_{mn} are known functions of Ka and h/a, and where each unknown occurs outside as well as inside the sign of summation. This simultaneous system involving the two unknown sets p_{2n} and q_{2n} can be reduced in several ways to the standard form involving only a single set. The simplest is merely to write $q_{2n}=p_{2n-1}$; this is convenient for numerical work. Alternatively, by adding i times (2.33) to (2.32), a single set for $p_{2m}+iq_{2m}$ is obtained; this is convenient for theoretical work on the convergence of the system. Or one may note that q_{2n} occurs in all the equations (2.32) only in the combination $\Sigma(k_0a)^{2n}q_{2n}/(2n)!$, and p_{2n} in (2.33) in a similar combination; these combinations may be treated as additional parameters (see Ursell 1950, p. 147). Any one of these methods leads to a system of the singly-infinite form

$$p_m^*+\sum_{n=1}^{\infty} a_{mn}^*p_n^*=\alpha_m^* \quad (m=1,2,3,\ldots),$$

where again each unknown occurs outside as well as inside the sign of summation. A system of this form corresponds to Fredholm's integral equation of the second kind and has a similar theory if certain convergence conditions are satisfied, e.g. if $\Sigma\Sigma|a_{mn}^*|^2$ and $\Sigma|\alpha_m^*|^2$ are convergent. These conditions are already known to hold for infinite depth except for those values of Ka, if any, where the infinite determinant vanishes and for which the source term is not needed in the expansion. It can be shown that the same convergence conditions also hold for finite depth but the proof will not be given here. It follows that the potential $\phi(x,y;t)$ can indeed be expanded in the form (2.26).

2.4. *The amplitude ratio*

When all the p_{2n} and q_{2n} are known, A and B can be found from (2.30) and (2.31). The dimensionless parameter J defined at the beginning of §2.3 can also be expressed in terms of p_{2n} and q_{2n}. For the surface displacement is

$$g^{-1}(\partial/\partial t)\{(gb/\pi\sigma J)\,\phi(x,0;t)\}$$

which tends to

$$\frac{b}{\pi J}\frac{2\pi\cosh^2 k_0h}{2k_0h+\sinh 2k_0h}\Big[\sin(k_0|x|-\sigma t)\Big\{\operatorname{sech}^2 k_0h\sum_{n=1}^{\infty}\frac{(k_0a)^{2n}}{(2n)!}q_{2n}\Big\} - \cos(k_0|x|-\sigma t)\Big\{1+\operatorname{sech}^2 k_0h\sum_{n=1}^{\infty}\frac{(k_0a)^{2n}}{(2n)!}p_{2n}\Big\}\Big]$$

as $|x|$ tends to infinity—see (2.15), (2.23), (2.24). By the definition of b this has amplitude b, and it follows that

$$J=\frac{2\cosh^2 k_0h}{2k_0h+\sinh 2k_0h}\Big[\Big\{\operatorname{sech}^2 k_0h\sum_{n=1}^{\infty}\frac{(k_0a)^{2n}}{(2n)!}q_{2n}\Big\}^2 + \Big\{1+\operatorname{sech}^2 k_0h\sum_{n=1}^{\infty}\frac{(k_0a)^{2n}}{(2n)!}p_{2n}\Big\}^2\Big]^{\frac{1}{2}}, \tag{2.34}$$

which evidently tends to 1 as Kh tends to infinity. It is now possible to find the amplitude ratio (wave amplitude at infinity)/(amplitude of motion of the cylinder), for from (2.27) the vertical velocity of the circle is

$$\frac{gb}{\pi\sigma Ja}(A\cos\sigma t + B\sin\sigma t),$$

which has amplitude $(gb/\pi\sigma Ja)\sqrt{(A^2+B^2)}$, the displacement has amplitude $(gb/\pi\sigma^2 Ja)\sqrt{(A^2+B^2)} = (b/\pi KaJ)\sqrt{(A^2+B^2)}$, and the amplitude ratio is seen to be $\pi KaJ/\sqrt{(A^2+B^2)}$, where J is given by (2.34) and A and B by (2.30) and (2.31).

2.5. *The vertical force on the cylinder*

When the cylinder oscillates vertically, the hydrostatic upward force on it per unit length is evidently $2\rho g a y_*$ (where y_* is the instantaneous downward vertical displacement). There is also a hydrodynamic force, obtained by resolving and integrating over the cylinder the dynamic pressure, which is of magnitude $-\rho(\partial/\partial t)\{(gb/\pi\sigma J)\,\phi(x,y;t)\}$. Thus the downward hydrodynamic force per unit length is

$$\begin{aligned} F_y &= \frac{\rho g b}{\pi\sigma J}\int_{-\frac{1}{2}\pi}^{\frac{1}{2}\pi}\frac{\partial\phi}{\partial t}a\cos\theta\,d\theta \\ &= -\frac{\rho g a b}{\pi J}\left[M\left(Ka,\frac{h}{a}\right)\sin\sigma t + N\left(Ka,\frac{h}{a}\right)\cos\sigma t\right], \end{aligned}$$

where from (2.26)

$$\begin{aligned} M\left(Ka,\frac{h}{a}\right) &= \int_{-\frac{1}{2}\pi}^{\frac{1}{2}\pi}F(a\sin\theta, a\cos\theta)\cos\theta\,d\theta \\ &\quad - \sum_{n=1}^{\infty}\frac{a^{2n}}{2n}\left[p_{2n}\int_{-\frac{1}{2}\pi}^{\frac{1}{2}\pi}F_{2n}(a\sin\theta, a\cos\theta)\cos\theta\,d\theta\right. \\ &\qquad \left. - q_{2n}\int_{-\frac{1}{2}\pi}^{\frac{1}{2}\pi}f_{2n}(a\sin\theta, a\cos\theta)\cos\theta\,d\theta\right], \end{aligned}$$

and

$$\begin{aligned} N\left(Ka,\frac{h}{a}\right) &= -\int_{-\frac{1}{2}\pi}^{\frac{1}{2}\pi}f(a\sin\theta, a\cos\theta)\cos\theta\,d\theta \\ &\quad + \sum_{n=1}^{\infty}\frac{a^{2n}}{2n}\left[p_{2n}\int_{-\frac{1}{2}\pi}^{\frac{1}{2}\pi}f_{2n}(a\sin\theta, a\cos\theta)\cos\theta\,d\theta\right. \\ &\qquad \left. + q_{2n}\int_{-\frac{1}{2}\pi}^{\frac{1}{2}\pi}F_{2n}(a\sin\theta, a\cos\theta)\cos\theta\,d\theta\right]. \end{aligned}$$

It is traditional to resolve the force into two components, in phase respectively with the velocity and the acceleration of the vertical motion of the cylinder. We have

$$\begin{aligned} F_y &= -(M\sin\sigma t + N\cos\sigma t)\frac{\rho g a b}{\pi J} \\ &= -\frac{NA+MB}{A^2+B^2}(A\cos\sigma t + B\sin\sigma t)\frac{\rho g a b}{\pi J} \\ &\quad -\frac{MA-NB}{A^2+B^2}(A\sin\sigma t - B\cos\sigma t)\frac{\rho g a b}{\pi J}. \end{aligned}$$

Over a cycle the former component does work which is carried away to infinity by the waves, and its coefficient is easily expressed in terms of the wave amplitude at infinity. The latter component is

$$-\tfrac{1}{2}\pi\rho a^2 \frac{2}{\pi}\frac{NB-MA}{A^2+B^2} \times (\text{acceleration of cylinder}),$$

and we define the dimensionless virtual-mass coefficient c_F by

$$c_F\left(Ka, \frac{h}{a}\right) = \frac{2}{\pi}\frac{NB-MA}{A^2+B^2},$$

which depends on the frequency. The notion of virtual mass is natural for a body oscillating in an inviscid fluid without a free surface, where the force is always proportional to the acceleration and where the virtual mass is thus independent of the frequency. In wave problems the resolution is artificial.

2.6. *Numerical results*

The amplitude ratio and virtual-mass coefficient which are functions of the two variables Ka and h/a were computed for $0{\cdot}15 \leqslant Ka \leqslant 6{\cdot}0$ and for $h/a = 2, 4, 10$ and ∞. The computations were made on the IBM-704 digital computer at the Computation Center of the Massachusetts Institute of Technology. Computations were first made for infinite depth, all unknowns up to p_{32} and q_{32} were retained. Since for infinite depth the computation of the p's is independent of the computation of the q's, this meant the solution of two systems of 16 linear equations, each with 16 unknowns. The results were checked against a similar calculation retaining only $8p$'s and $8q$'s, and against the results of the manual computation in Ursell (1949), and agreement to 3 significant figures was observed. Computations were then made for the other values of h/a, retaining $8p$'s and $8q$'s. As an additional check, values of the two integrals $G_{2s+1}(v)$ and $\mathscr{F}_{2s+1}(v)$ obtained manually were compared both with results from the IBM-704 and with uniform asymptotic expansions (not given here), valid for large v and s. To avoid the infinities on the real u-axis, see (2.13) and (2.22), the integrals were transformed by moving the line of integration to $\arg u = \frac{1}{4}\pi$ in the complex u-plane.

The computed curves of the amplitude ratio against Ka for the four values of h/a are shown in figure 2. The values for $h/a = 10$ and $h/a = \infty$ effectively coincide, and it appears that the effect of finite depth on the amplitude ratio is not appreciable until the ratio of depth to cylinder radius is equal to 2. For comparison, Grim's curve (1953) is also shown in figure 2 for $h = \infty$. The computed curves of the virtual-mass coefficient c_F against Ka for the four values of h/a are shown in figure 3. It is known that c_F tends to infinity like a multiple of $\ln(1/Ka)$ when Ka tends to zero. The dependence of c_F on h/a is seen to be stronger than the dependence of the amplitude ratio. However, the curves for $h/a = \infty$ and $h/a = 10$ again coincide very nearly. Grim's curve, for $h = \infty$, is also shown for comparison.

3. Description of experimental apparatus

3.1. *Wave channel and general arrangement*

The experiments were made in the wave channel of the Hydrodynamics Laboratory of the Massachusetts Institute of Technology. The channel is 100 ft. long, with a rectangular section $2\frac{1}{2}$ ft. wide and 3 ft. high, with glass walls and bottom. The clear length available for the present study was limited to about 70 ft. with a horizontal bottom. The cylinder generating the waves was located at the middle of the clear length with its axis perpendicular to the side walls of the channel; the clearances between the ends of the cylinder and the side walls were about $\frac{1}{4}$ in. The wave energy travelling away from the cylinder was partially absorbed by two similar wave absorbers made of aluminium wool, near the two ends of the clear length of the channel and placed symmetrically with respect to the cylinder. An effort was made to make the experiment symmetrical about the vertical plane through the axis of the cylinder. The arrangement is shown schematically in figure 1.

3.2. *Wave-making unit*

This consisted of three parts, a drive unit, a linkage and a cylinder (see figure 1). The drive unit had a $\frac{1}{2}$ horsepower alternating-current variable-speed motor coupled with a 12:1 reducing gear giving an output speed range from 0 to 230 revolutions per minute. A flywheel of diameter 1 ft. was mounted on the output shaft of the reducing gear and carried an eccentric block which was connected by a rod to one of the arms fixed to the steel shaft of the linkage. The shaft, $1\frac{1}{2}$ in. in diameter and $3\frac{1}{2}$ ft. long, was supported with its axis normal to the channel walls by two pillar blocks bolted on the top flanges of the walls. It carried three lever arms, each 1 ft. long and each with one end rigidly fixed to the shaft. One of the arms was connected to the flywheel, the other two supported the cylinder by means of supporting rods. The stroke of the cylinder could be varied over a range of 0 to 6 in. by changing the position of the eccentric block on the flywheel.

The two water-tight cylinders, one of 6 in. and one of 12 in. outside diameter, were made of Plexiglass tubing of $\frac{1}{8}$ in. wall-thickness. Each cylinder was of length $29\frac{1}{2}$ in., of semicircular section with vertical sides extended 4 in. above the water surface. In the experiments the axis of the cylinder in use was normal to the side walls of the channel, and there was a gap of $\frac{1}{4}$ in. between the ends of the cylinder and the channel walls. The position of the cylinder could be adjusted by replacing the supporting rods by rods of different lengths. The hollow cylinder was filled with several sand bags so that its weight was equal to the buoyant force when its semicircular section was fully immersed in water. A coil assembly of the linear variable differential transformer (see §3.5) for measuring the displacement of the cylinder was installed on the cover plate of the cylinder. Guiding devices were provided to ensure vertical oscillation of the cylinder.

3.3. *Wave absorber*

A permeable type of absorber with a total length of $9\frac{1}{2}$ ft. made of aluminium wool was located at each end of the channel to dissipate the energy of the wave

motion generated in the middle of the channel. Each absorber had two sections. The first section was a cage $4\frac{1}{2}$ ft. long, $2\frac{1}{2}$ ft. wide, and $2\frac{1}{2}$ ft. high, made of wire screen and divided into three vertical compartments each $1\frac{1}{2}$ ft. long and packed with aluminium wool. The density of packing increased with distance from the wave-maker, the total weight of aluminium wool in the three compartments being 2, 4 and 6 lb., respectively. Behind the cage there was a pile of aluminium sausages, each 5 ft. long and about 10 in. in diameter, laid lengthwise in the channel. Two vertical rigid walls were placed behind the absorbers for symmetry. With these absorbers the reflexion in the experiments did not exceed 20 % and was usually less than 10 %.

3.4. *Wave-height gauge*

Two resistance-type wave-height probes were mounted on movable carriages (see figure 1) to measure the wave height at different locations along the channel. The sensing element of each probe, composed of two platinum wires 0·008 in. in diameter and about 1 ft. long, was connected to one branch of a bridge circuit. When the elevation of the water surface changed, the immersed length of the wire also changed. In fact, since the resistance of the gauge is proportional to the length of the wire above the water surface, the current flowing through it varies linearly (very nearly) as the displacement of the water surface from its mean position. The output signal was amplified and recorded on a Sanborn recorder.

Each carriage could be driven along the channel at a constant speed of $\frac{1}{4}$ in. per second, and a continuous record was obtained of the wave height as a function of time and distance. The distance of each gauge from the axis of the cylinder was recorded by a remote electric marker connected to the recorder.

3.5. *Linear variable differential transformer*

This transformer (Linearsyn Model S 2) measured the vertical displacement of the cylinder from its mean position. It converts the displacement into an electrical signal directly proportional to the displacement. This device has two parts, a coil assembly $11\frac{1}{8}$ in. long, with an inner diameter of 0·312 in. and an outer diameter of $\frac{3}{4}$ in., and a magnetic core of diameter $\frac{1}{4}$ in. and length 6 in. which can slide into the coil assembly. The magnetic core was screwed to a point-gauge stem clamped to a beam spanning the channel above the water; the coil assembly was fixed to the cylinder and followed its motion. The displacement of the coil assembly was also recorded by the Sanborn recorder. The transformer had a full range of stroke of 4 in. and an excitation voltage of 6 V.

4. Analysis of wave reflexion

In the mathematical theory of § 2 it was assumed that the wave channel is infinitely long, or that absorption of wave energy at the ends of the channel is complete. In practice the absorption is incomplete (the amplitude reflexion coefficient is at least a few percent, and in the present series of measurements is sometimes as much as 20 %); and unless it is corrected for, it is one of the most serious limitations on experimental accuracy. This difficulty has been discussed at length in I, § 4.1, where it is shown how it can be overcome when the waves

are generated by a vertical or nearly vertical wave-maker, but the method then used took advantage of the simple geometry. Here we shall have to proceed more elaborately.

In the following analysis it will be assumed that the motion is exactly symmetrical about $x = 0$. It is then sufficient to consider the region $x > 0$ as will henceforth be done. It will also be assumed that the effect of viscous attenuation is much smaller than the effect of partial reflexion (see I, §§ 4.2, 7.2).

Let ϕ_1 denote the wave motion as measured. At a distance from both the cylinder and the absorber, the motion is effectively the superposition of two regular wave trains, and there the downward surface displacement is (with a suitable choice of time origin)

$$\eta_1 = A_1 \sin(k_0 x - \sigma t) - A_2 \sin(k_0 x + \sigma t + \delta), \tag{4.1}$$

where A_1, A_2 and δ can be found by measuring the variation of wave amplitude along the channel, and where $A_1 \gg A_2$. The vertical velocity of the cylinder is denoted by

$$v_1 = -l\sigma \cos(\sigma t + \epsilon). \tag{4.2}$$

The wave amplitude at distance x is easily seen to be

$$\sqrt{(A_1^2 + A_2^2 + 2A_1 A_2 \cos(2k_0 x + \delta))}. \tag{4.3}$$

From the motion ϕ_1, another dynamically possible motion can be derived by reversing the sign of t. (It is in this argument that the influence of viscosity is neglected.) More precisely, we replace t by $-t - (\delta/\sigma)$ to obtain a motion ϕ_2. Then, in an obvious notation, we have

$$\eta_2 = A_2 \sin(k_0 x - \sigma t) - A_1 \sin(k_0 x + \sigma t + \delta),$$

$$v_2 = -l\sigma \cos(\sigma t + \delta - \epsilon).$$

Now let us consider the composite motion $\phi_3 = \phi_1 - (A_2/A_1)\phi_2$. Then the surface displacement is

$$\eta_3 = A_1\{1 - (A_2/A_1)^2\} \sin(k_0 x - \sigma t), \tag{4.4}$$

and the velocity of the cylinder is

$$\begin{aligned} v_3 &= -l\sigma\{\cos(\sigma t + \epsilon) - (A_2/A_1)\cos(\sigma t + \delta - \epsilon)\} \\ &= -l\sigma\alpha \cos(\sigma t + \delta_1), \quad \text{say,} \end{aligned}$$

where $\alpha \cos\delta_1 = \cos\epsilon - (A_2/A_1)\cos(\delta - \epsilon)$ and $\alpha \sin\delta_1 = \sin\epsilon - (A_2/A_1)\sin(\delta - \epsilon)$. Equation (4.4) shows that ϕ_3 satisfies the condition of complete absorption, and the amplitude ratio for ϕ_3 is

$$\frac{A_1}{l\alpha}\left\{1 - \left(\frac{A_2}{A_1}\right)^2\right\} = \frac{A_1}{l} \frac{\{1 - (A_2/A_1)^2\}}{\{1 + (A_2/A_1)^2 - 2(A_2/A_1)\cos(2\epsilon - \delta)\}^{\frac{1}{2}}}. \tag{4.5}$$

This is the quantity which is to be compared with the theory of § 2, and we now see how it is related to the amplitudes and phases of the actual measured motion ϕ_1.

5. Methods of measurement

In order to verify the validity of the assumptions of the linearized theory, measurements were made to determine the wave amplitude when the circular cylinder was given a forced heaving motion. The analysis of §4 shows how the amplitude in a hypothetical channel of infinite length may be deduced from measurements on the actual wave motion in a channel of finite length. The following measurements are needed for the amplitude ratio (see equation (4.5)): (i) water depth h; (ii) wavelength $L = 2\pi/k_0$; (iii) amplitude A_1 of the incident wave, amplitude A_2 of the reflected wave, and relative phase δ (see equation (4.1)); (iv) amplitude l and phase ϵ of the cylinder motion (see equation (4.2)).

5.1. *Water depth*

This was measured directly (in feet) with a wooden scale immersed through the still-water surface. For the range of water depths involved, the error was less than 1 %. The consequent error in the amplitude ratio was thus negligibly small (much less than 1 %).

5.2. *Wavelength*

This was obtained indirectly from measurements of the wave period T by use of the formulae

$$(2\pi/T)^2 = gk_0 \tanh k_0 h, \quad \text{and} \quad L = 2\pi/k_0.$$

An electric timer which reads to the nearest 0·02 sec was used to record the time elapsed for 20 oscillations of the cylinder. The average value of three measurements (one at the beginning of the run, one at the end, and one in between) was adopted. It was found that the motor speed was nearly constant, the maximum difference in the three values being less than 0·5 %. For relatively deep water the consequent error in the wavelength would be less than 1 %.

5.3. *The wave amplitudes and the wave phase*

These are obtained from the variation of wave amplitude along the channel (see equation (4.3)). Two resistance gauges, of the type described in §3, were calibrated statically by being held in still water at known levels. Changes in the immersed length were read on a vernier scale to 0·1 mm. The gauges were also calibrated dynamically, being given a vertical periodic motion of known amplitude in still water. The maximum difference between the static and the dynamic calibrations was about 0·03 cm, of the order of 3 % of the amplitude. It was therefore thought sufficient to make only static calibrations throughout the experiments.

In each run the two gauges were placed one on each side of the cylinder at 20 ft. from its axis, and when the wave motion had reached a steady state they were made to move slowly towards the cylinder. Since the wave motion approximates to the sum of two wave trains only at some distance from both the cylinder and the absorbers, measurements were confined on each side to a range of 7 ft., namely, from 13 to 20 ft. from the axis of the cylinder. (Note that for the analysis of §4, measurements over at least half a wavelength are needed.) The record of

wave height against position (see equation (4.3)) is the wave-height envelope, from which the arithmetic means of the wave-amplitude maxima and similarly of the minima on either side of the cylinder were found. The assumption of symmetry was checked by comparing the mean maxima and mean minima from both sides, and it was found that the discrepancy was less than 4 % in most runs. The mean of the values on the two sides was then taken. The average of the wave-amplitude maxima was used as an estimate for $A_1 + A_2$; similarly the minima were used to give an estimate for $A_1 - A_2$. The angular phase δ was determined by measuring the distances of the wave height maxima from the cylinder, subtracting an appropriate integral multiple of $\frac{1}{2}L$, and dividing by $L/4\pi$ (see equation (4.3)). An average was taken for each side of the cylinder, and it was found that the discrepancy between the mean phases on the two sides was larger than for the amplitudes, particularly for short-period waves as might have been expected. But for such waves the reflexion was small, and the uncertainty in δ was of little consequence. Viscous attenuation of wave amplitude was neglected throughout.

5.4. *Amplitude and phase of the oscillating cylinder*

The amplitude l of the oscillating cylinder was measured in centimetres with a linear variable differential transformer. The transformer was calibrated by moving the magnetic core up and down in the coil assembly. The movement could be read from a vernier to 0·1 mm, and was recorded on the Sanborn recorder simultaneously with the wave-height record. It was found that the cylinder motion was of nearly constant amplitude throughout each run, and that its form was nearly sinusoidal. (For an account of the effect of higher harmonics, see I, §4.3.)

The phase ϵ was measured by moving the wave-height probe along the channel until the wave motion was either in phase or 180° out of phase with the cylinder motion (both motions being recorded on the Sanborn recorder). It is easily shown that the horizontal co-ordinate x at such points satisfies

$$A_1 \sin(k_0 x + \epsilon) - A_2 \sin(k_0 x + \delta - \epsilon) = 0;$$

and since A_2/A_1 is small, ϵ differs from $-k_0 x$ by a multiple of π, very nearly. Here x is again the distance from the axis of the cylinder, and $k_0 = 2\pi/L$ is the value calculated from the period.

In calculating the phase angles ϵ and δ, it seems that a large error might be committed, since the distance from the cylinder (which may be several wavelengths) enters into both calculations. Actually the angle which appears in the formula (4.5) for the amplitude is $2\epsilon - \delta$, and it is easily seen that this depends (to our approximation) only on the relative distance between two points, not on their absolute distance from the cylinder axis.

6. The amplitude ratio: comparison of theory and experiment

Measurements were made for two cylinders with diameters of 6 and 12 in. Each cylinder was immersed in water 10·5 and 22·75 in. deep. Thus there were four ratios of water depth to cylinder radius, namely 7·58, 3·79, 3·50 and 1·75. For each fixed value of this ratio measurements were made for different

wave periods and also for different strokes of the cylinder motion. The stroke of the cylinder was kept small to simulate the small-amplitude wave of the theory, and yet was large enough to generate waves with height which could be measured with sufficient accuracy (maximum error about 3 %) using the present apparatus. The methods of measurement were described in detail in §5.

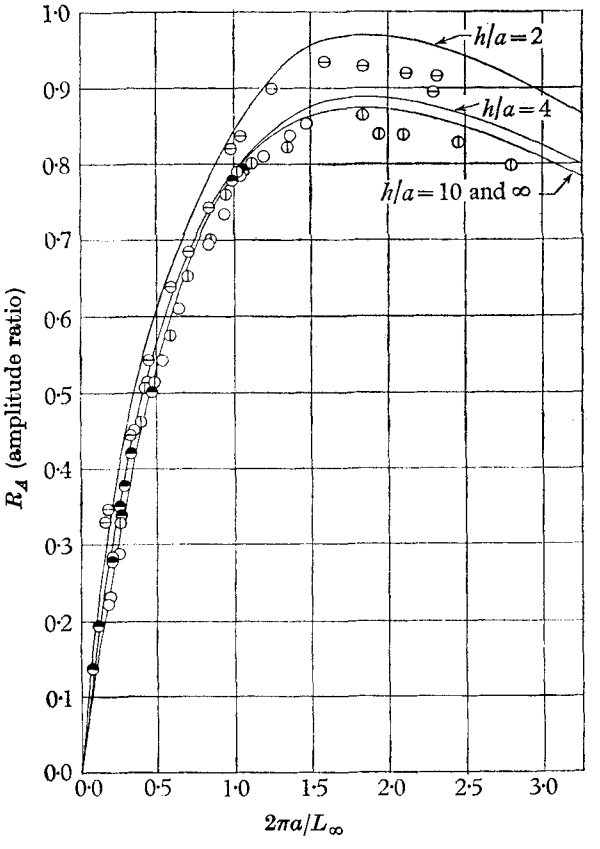

FIGURE 4. Comparison of theoretical and measured amplitude ratios. ——, Computed curve. h = water depth; a = radius of cylinder; L_0 = deep-water wavelength.

measured	h/a	a (in.)
○	7·58	3
◑	3·78	6
●	3·50	3
⊖	1·75	6

The measurements are summarized in Appendix B, tables 1 to 4. Experimental results were limited to values of Ka less than 3. At higher frequencies water in the gaps between the walls of the channel and the ends of the cylinder tended to oscillate violently even when damping screens were put in the gap, and the recorded wave-height envelope was very irregular. No attempt was made to analyse such data.

The amplitude ratio, corrected for wave reflexion as in §4, is plotted in figure 4 which also shows the results of the theoretical computations. (Although the values of h/a in the experiments do not coincide with the values of h/a in the theory, it has not been thought worth while to carry out any formal interpolation.) The discrepancy between experiment and theory is seen to be systematic but small. The experimental points in general lie below the theoretical values, but the discrepancy is usually less than about 5%. (A similar discrepancy found in I could be partly attributed to finite wave steepness. We have not investigated the effect of steepness here.) This agreement between theory and experiment on amplitude ratio is believed to be as good as can be expected with the present experimental arrangement.

For comparison a few points (not shown in figure 4) were also analysed by a simpler method, the amplitude ratio being taken as A_1/l instead of formula (4.5). This can be justified as follows: If $(A_2/A_1)^2$ is neglected, formula (4.5) is nearly

$$\frac{A_1}{l}\left[1+\frac{A_2}{A_1}\cos(2\epsilon-\delta)\right],$$

which has mean value A_1/l when δ varies between 0 and 2π. Thus if the length of the channel is regarded as an unknown multiple of the wavelength, which means that δ is regarded as random, the appropriate value for the amplitude ratio is A_1/l. It was found that the scatter of the points obtained in this way was noticeably greater than in figure 4. Thus if experimental accuracy is desired in a channel of finite length it appears that the complications of the preceding analysis cannot be avoided.

7. Conclusion

We have shown how the mathematical linearized theory of the heaving cylinder can be extended to a channel of finite constant depth. We have also shown how wave measurements in a channel of finite length can be analysed so as to give the wave amplitude in a channel of infinite length when the experiment is arranged to be symmetrical about the vertical plane through the axis of the cylinder.

The agreement between theory and experiment for the wave amplitude was found to be very satisfactory. No experiments have yet been made on the virtual mass coefficient, but Porter (1960) has calculated and measured the pressure distribution on a heaving circular cylinder. The agreement which he has obtained between theory and experiment is surprisingly good, considering that he has not apparently made any allowance for the finite length of the channel (nor for finite depth though this is less important). A non-symmetrical experiment, the partial reflexion of a wave train by a fixed circular cylinder, has been described by Dean & Ursell (1959). Amplitudes and forces were measured and compared with theory. Naturally the measurements were more numerous and the analysis more complicated than for a symmetrical experiment.

This investigation was sponsored by the Office of Naval Research, United States Department of the Navy, under Contract no. Nonr-1841 (44).

REFERENCES

DEAN, R. G. & URSELL, F. 1959 Interaction of a fixed semi-immersed circular cylinder with a train of surface waves. *M.I.T. Hydrodynamics Laboratory, Tech. Rep.* no. 37.

GRIM, O. 1953 Berechnung der durch Schwingungen eines Schiffskörpers erzeugten hydrodynamischen Kräfte. *Jb. schiffbautech. Ges.* **47**, 277–96.

JOHN, F. 1950 On the motion of floating bodies. II. *Comm. Pure Appl. Math.* **3**, 45–101.

PORTER, W. R. 1960 Pressure distributions, added-mass, and damping coefficients for cylinders oscillating in a free surface. *Inst. Engng Res., Univ. of California, Berkeley, Series* 82, Issue 16.

THORNE, R. C. 1953 Multipole expansions in the theory of surface waves. *Proc. Camb. Phil. Soc.* **49**, 707–16.

URSELL, F. 1949 On the heaving motion of a circular cylinder on the surface of a fluid. *Quart. J. Mech. Appl. Math.* **2**, 218–31.

URSELL, F. 1950 Surface waves on deep water in the presence of a submerged circular cylinder. I. *Proc. Camb. Phil. Soc.* **46**, 141–52.

URSELL, F. 1953 Short surface waves due to an oscillating immersed body. *Proc. Roy. Soc.* A, **220**, 90–103.

URSELL, F. 1954 Water waves generated by oscillating bodies. *Quart. J. Mech. Appl. Math.* **7**, 427–37.

URSELL, F., DEAN, R. G. & YU, Y. S. 1959 Forced small-amplitude water waves: a comparison of theory and experiment. *J. Fluid Mech.* **7**, 33–52.

WHITTAKER, E. T. & WATSON, G. N. 1927 *Modern Analysis*, 4th ed. Cambridge University Press.

Appendix A. Note on the expansion of the wave-source potential

Let the term (2.10) be denoted by $F_1(x, y)$. Then

$$F_1(x,y) = \mathscr{P}\int_0^\infty \frac{e^{-ky}\cos kx\,dk}{K-k} = \mathrm{Re}\,\mathscr{P}\int_0^\infty \frac{e^{-v\eta+iv\xi}}{1-v}\,dv$$

$$= \mathrm{Re}\,\mathscr{P}\int_0^\infty \frac{e^{-v\zeta}}{1-v}\,dv = \mathrm{Re}\,f_1(\zeta), \quad \text{say,}$$

where $$\xi = Kx, \quad \eta = Ky, \quad \text{and} \quad \zeta = \eta - i\xi = Kre^{-i\theta}.$$

Clearly $f_1(\zeta)$ is related to the exponential-integral function and is analytic in $\eta > 0$. Suppose first that ζ is real and positive. Then

$$e^{\zeta}f_1(\zeta) = -\mathscr{P}\int_{-\zeta}^\infty e^{-w}\frac{dw}{w};$$

also Euler's constant $\gamma = 0{\cdot}5772\ldots$ is given by

$$\gamma = \int_0^1 \frac{1-e^{-w}}{w}\,dw - \int_1^\infty \frac{e^{-w}}{w}\,dw.$$

Then, by simple algebra,

$$e^{\zeta}f_1(\zeta) - \gamma - \int_0^\zeta \frac{e^w-1}{w}\,dw = \int_1^\zeta \frac{dw}{w} = \ln\zeta,$$

whence

$$f_1(\zeta)-\gamma e^{-\zeta}-e^{-\zeta}\ln\zeta = e^{-\zeta}\int_0^{\zeta}\frac{e^w-1}{w}dw = -\int_0^1\frac{e^{-\zeta}-e^{-\zeta u}}{1-u}du, \quad \text{where} \quad u=1-\frac{w}{\zeta},$$

$$= -\sum_1^{\infty}\frac{(-\zeta)^m}{m!}\int_0^1\frac{1-u^m}{1-u}du$$

$$= -\sum_1^{\infty}\frac{(-\zeta)^m}{m!}\int_0^1(1+u+u^2+\ldots+u^{m-1})\,du,$$

and so
$$f_1(\zeta) = \gamma e^{-\zeta}+e^{-\zeta}\ln\zeta-\sum_1^{\infty}\frac{(-\zeta)^m}{m!}\left(\frac{1}{1}+\frac{1}{2}+\ldots+\frac{1}{m}\right).$$

This relation has been proved on the assumption that ζ is real and positive, but both sides are analytic functions when $\eta > 0$, and so the relation holds at least in the half-plane $\eta > 0$, and in fact in the whole ζ-plane cut along the negative η-axis. On putting $\zeta = Kre^{-i\theta}$ and taking the real part, it is found that

$$F_1(x,y) = \ln Kr\sum_0^{\infty}\frac{(-Kr)^m}{m!}\cos m\theta-\theta\sum_0^{\infty}\frac{(-Kr)^m}{m!}\sin m\theta$$

$$+\gamma\sum_0^{\infty}\frac{(-Kr)^m}{m!}\cos m\theta-\sum_1^{\infty}\frac{(-Kr)^m}{m!}\left(\frac{1}{1}+\frac{1}{2}+\ldots+\frac{1}{m}\right)\cos m\theta.$$

Appendix B. Summary of experimental results

The following notation is used:

T = measured period of waves;

$L_\infty = gT^2/2\pi$, deep-water wavelength calculated from the period;

$2l$ = stroke of vertical motion of cylinder;

$Ka = 2\pi a/L_\infty$, where a is the cylinder radius;

$H_{\max}$, $H_{\min}$ = maximum and minimum wave heights from crest to trough;

$A_1 = \frac{1}{4}(H_{\max}+H_{\min})$;

$A_2 = \frac{1}{4}(H_{\max}-H_{\min})$;

δ = wave phase (see §5.3);

ϵ = phase of cylinder motion (see §5.4);

R_A = amplitude ratio (see equation (4.5)).

Run no.	L_∞ (ft.)	$2l$ (cm)	H_{max} (cm)	H_{min} (cm)	A_2/A_1	$2\epsilon-\delta$ (π rad)	Ka	R_A
1	4·40	2·46	1·12	1·01	0·057	1·37	0·357	0·451
2	3·65	2·46	1·28	1·22	0·024	1·83	0·431	0·514
3	2·98	2·46	1·45	1·30	0·057	0·63	0·527	0·543
4	2·46	2·46	1·58	1·43	0·030	1·68	0·639	0·610
5	1·87	2·46	1·95	1·64	0·083	0·67	0·834	0·695
6	1·32	1·82	1·60	1·34	0·088	0·45	1·19	0·810
7	1·07	1·86	1·78	1·49	0·092	0·56	1·47	0·852
8	6·20	3·03	1·05	0·85	0·105	1·74	0·253	0·289
9	9·00	3·03	0·91	0·63	0·19	1·35	0·175	0·223
10	8·20	3·03	0·89	0·67	0·105	1·71	0·192	0·267
11	9·10	3·03	0·94	0·63	0·19	1·38	0·173	0·231
12	7·61	3·03	0·96	0·76	0·12	0·41	0·206	0·286
13	1·67	2·15	1·79	1·59	0·060	1·04	0·940	0·735
14	1·51	1·56	1·27	1·09	0·076	0·59	1·04	0·765
15	1·15	1·67	1·44	1·06	0·15	1·74	1·37	0·839

TABLE 1. Experimental results for $h/a = 7{\cdot}58$, $a = 3$ in.

Run no.	L_∞ (ft.)	$2l$ (cm)	H_{max} (cm)	H_{min} (cm)	A_2/A_1	$2\epsilon-\delta$ (π rad)	Ka	R_A
1	2·80	1·31	1·13	0·90	0·104	0·30	1·12	0·801
2	1·50	1·40	1·26	1·08	0·052	0·41	2·10	0·838
3	1·72	1·41	1·26	1·07	0·079	0·26	1·83	0·864
4	3·08	1·31	1·09	0·96	0·068	0·39	1·02	0·791
5	7·67	2·65	1·44	1·30	0·053	0·57	0·410	0·507
6	12·1	2·68	1·01	0·73	0·103	0·39	0·260	0·330
7	8·00	2·66	1·24	1·03	0·090	0·04	0·393	0·462
8	6·49	2·66	1·40	1·18	0·110	0·27	0·484	0·513
9	5·42	2·66	1·53	1·39	0·048	0·02	0·580	0·575
10	4·47	2·66	1·88	1·72	0·046	0·80	0·703	0·652
11	3·70	2·66	2·06	1·76	0·080	1·43	0·850	0·700
12	3·31	2·67	2·29	2·00	0·069	0·84	0·950	0·760
13	1·62	1·97	1·69	1·46	0·073	1·75	1·95	0·838
14	2·33	1·85	1·61	1·41	0·066	0·42	1·35	0·823
15	1·12	2·06	1·77	1·51	0·080	1·55	2·80	0·799
16	1·28	2·06	1·80	1·59	0·062	1·59	2·45	0·827

TABLE 2. Experimental results for $h/a = 3{\cdot}78$, $a = 6$ in.

Run no.	L_∞ (ft.)	$2l$ (cm)	H_{max} (cm)	H_{min} (cm)	A_2/A_1	$2\epsilon-\delta$ (π rad)	Ka	R_A
1	1·46	2·38	2·06	1·65	0·113	1·16	1·07	0·792
2	1·61	2·38	1·97	1·71	0·073	0·42	0·976	0·781
3	3·33	2·30	1·30	1·11	0·079	0·69	0·471	0·501
4	4·86	2·30	0·97	0·87	0·053	1·95	0·323	0·421
5	5·99	2·30	0·80	0·69	0·073	0·28	0·263	0·338
6	5·06	3·24	1·24	1·17	0·029	1·85	0·283	0·377
7	6·20	3·24	1·15	1·02	0·062	1·21	0·253	0·349
8	7·25	3·24	1·01	0·80	0·114	0·54	0·209	0·278
9	13·3	3·24	0·69	0·54	0·121	0·57	0·118	0·194
10	20·7	3·24	0·54	0·37	0·191	1·58	0·076	0·138

TABLE 3. Experimental results for $h/a = 3{\cdot}50$, $a = 3$ in.

Run no.	L_∞ (ft.)	$2l$ (cm)	H_{max} (cm)	H_{min} (cm)	A_2/A_1	$2\epsilon-\delta$ (π rad)	Ka	R_A
1	20·5	3·24	1·09	0·86	0·12	1·86	0·154	0·330
2	16·4	3·24	1·14	0·88	0·13	1·13	0·192	0·347
3	9·31	3·24	1·60	1·37	0·078	0·59	0·338	0·443
4	7·23	2·63	1·49	1·29	0·072	1·67	0·435	0·544
5	5·35	2·63	1·69	1·56	0·043	0·18	0·588	0·638
6	4·31	2·63	2·04	1·79	0·068	0·78	0·729	0·685
7	3·71	2·63	2·16	1·95	0·053	0·93	0·847	0·743
8	3·02	2·63	2·49	2·11	0·083	1·37	1·04	0·837
9	1·48	1·43	1·39	1·18	0·081	0·40	2·12	0·920
10	1·36	1·43	1·32	1·20	0·048	0·19	2·32	0·914
11	2·52	1·31	1·26	1·05	0·095	0·30	1·25	0·900
12	1·37	1·43	1·28	1·15	0·049	1·90	2·30	0·894
13	1·72	1·92	1·90	1·67	0·066	0·45	1·83	0·928
14	1·99	1·91	1·83	1·65	0·050	1·56	1·58	0·934
15	3·16	1·83	1·57	1·44	0·042	0·18	0·994	0·820

TABLE 4. Experimental results for $h/a = 1{\cdot}75$, $a = 6$ in.